Biomedical Signal Processing and Control 86 (2023) 105254

Contents lists available at ScienceDirect

Biomedical Signal Processing and Control

journal homepage: www.elsevier.com/locate/bspc

SUVR quantification using attention-based 3D CNN with longitudinal Florbetapir PET images in Alzheimer's disease

R. Divya *, R. Shantha Selva Kumari, for the Alzheimer's Disease Neuroimaging Initiative[1]

Department of Electronics and Communication Engineering, Mepco Schlenk Engineering College, Sivakasi 626 005, Tamil Nadu, India

ARTICLE INFO

Keywords:
Alzheimer's disease
SUVR
PET
Attention
CNN

ABSTRACT

Purpose: Florbetapir PET images provide valuable information about the amount of amyloid deposition in the brain due to neurodegenerative diseases, which helps in the prognosis of patients. The purpose of this study is to develop a system that helps in the automatic amyloid quantification of the standard uptake value ratio so that drug treatments could be effectively determined.

Methods: 2647 Florbetapir PET images obtained from multiple centres of Alzheimer Disease Neuroimaging Initiative (ADNI) and an external dataset of 1413 scans from the Anti-Amyloid Treatment in Asymptomatic Alzheimer's study are used to design and test the proposed 3D CNN attention-based model to quantify the amyloid deposits. Only 80% of scans from the ADNI dataset are used to train the model. The remaining 20% of scans from ADNI and the external dataset are used for testing the trained model.

Results: The proposed model achieves a root mean square error of 0.0362 and a mean absolute error of 0.026 on separate hold-out test data from ADNI and a root mean square error of 0.058 and a mean absolute error of 0.044 Anti-Amyloid Treatment in Asymptomatic Alzheimer's study dataset. A graphical user interface is developed for the proposed model which will display a slice of the Florbetapir PET volume and its predicted standard uptake value ratio.

Conclusion: 3D CNN architecture with both spatial and channel attention provided better results when compared to models without attention. The proposed model proves to be an efficient tool in the automatic amyloid standard uptake value ratio quantification.

1. Introduction

Many elderly people are affected by progressive dementia due to Alzheimer's disease worldwide. Alzheimer's disease causes neurodegeneration in the brain which affects the day-to-day activities of the person. When this chronic disease progresses, it will lead to dementia and loss of bodily functions. There is uncertainty in the etiology of Alzheimer's disease, but the main biomarkers that are identified in Alzheimer's disease-affected persons are neurofibrillary tau tangles and beta-amyloid plaque deposition [1]. These biomarkers could be obtained in the cerebrospinal fluid and also by molecular imaging by PET. Research is going on to find a possible cure for this disease. Treatments are devised to reduce amyloid deposits between neurons in the brain [2]. Before the treatment, quantification of the amyloid deposition will help in a better prognosis of the disease.

Recent advancements in medical imaging have enabled the development of novel methods for medical image fusion, synthesis, and enhancement [3,4]. These methods utilize various techniques to improve the accuracy, and quality of medical imaging [5,6]. Enhancing the image, and reducing noise have the potential to significantly improve medical diagnosis and treatment [7,8]. Artificial intelligence comprising machine learning and deep learning is used in many fields like computer vision [9–11], image forgery detection [12], defect detection [13], style transfer [14], steganography [15], robotics [16,17] etc. Artificial intelligence also plays an active role in the medical field. In healthcare, machine learning techniques are used for classification, segmentation, and regression analysis based on handcrafted features [18]. Some studies have used grasshopper optimization technique [19],

* Corresponding author.
E-mail addresses: rdivya@mepcoeng.ac.in (R. Divya), rshantha@mepcoeng.ac.in (R. Shantha Selva Kumari).

[1] Data used in the preparation of this article were obtained from the Alzheimer's Disease Neuroimaging Initiative (ADNI) database (adni.loni.usc.edu). As such, the investigators within the ADNI contributed to the design and implementation of ADNI and/or provided data but did not participate in the analysis or writing of this report. A complete listing of ADNI investigators can be found at: http://adni.loni.usc.edu/wp-content/uploads/how_to_apply/ADNI_Acknowledgement_List.pdf.

https://doi.org/10.1016/j.bspc.2023.105254
Received 17 November 2022; Received in revised form 7 June 2023; Accepted 3 July 2023
Available online 11 July 2023
1746-8094/© 2023 Elsevier Ltd. All rights reserved.

Table 1
Details of the study participants.

Category ADNI (n = 2647)	CN (n = 1052)		MCI (n = 1195)		AD (n = 400)	
	Amyloid positive	Amyloid Negative	Amyloid positive	Amyloid Negative	Amyloid positive	Amyloid Negative
Number of images	322	730	603	592	345	55
Gender (F/M)	196/126	369/361	269/334	243/349	160/185	14/41
Age	77.10 ± 6.53	74.91 ± 7.18	75.44 ± 7.58	73.26 ± 8.27	76.21 ± 7.80	77.35 ± 7.21

swarm optimization techniques [20,21] and equilibrium optimization techniques [22,23] for medical image fusion. Deep learning techniques use neural networks to identify the disease-affected regions, for segmentation tasks, and detection of disease from behavioral and living environment data [24–27]. Significant works were done to classify Alzheimer's disease stages as cognitively normal, mild cognitive impairment, and dementia due to Alzheimer's disease using machine learning or deep learning [28–31] and to predict mini-mental state examination scores. Machine learning and deep learning algorithms are used with the PET images of Alzheimer's disease to reduce scan acquisition time [32], for image enhancement [33], and for the classification of amyloid positive and negative scans [34,35]. Some studies [36,37] used PET images to classify Alzheimer's disease progress from mild cognitive impairment.

Previously done research in the field found atrophy in the brain caused by Alzheimer's disease but the abnormal amyloid and tau proteins deposition occurs even before the atrophy occurs. Atrophy is best identified in the brain by using MRI images and metabolic changes in the brain are understood with the help of functional imaging. Fluorodeoxyglucose (FDG) PET images are used to recognize the glucose metabolism changes in the brain which helps in differentiating Alzheimer's disease from other diseases causing dementia. Medical imaging techniques like amyloid PET and tau PET are used to know the amount of amyloid and tau deposition respectively [38]. PET radiotracers like Florbetapir, Florbetaben, and Flutemetamol are used to know about the amyloid deposition level in the brain. These radiotracers attach themselves to the beta-amyloid plaques which could be identified in the PET imaging. When the standard uptake value ratio (SUVR) of amyloid deposition is above 0.78, the Florbetapir PET scan is positive or otherwise negative.

Amyloid PET scans improved the diagnosis of Alzheimer's disease by allowing early detection of the amyloid plaques that accumulate in the brain. Quantification of radiotracer uptake permits a more granular evaluation and potentially pinpoints key regions of the brain for classification. However, there are still some challenges and problems that need to be addressed in the classification of Alzheimer's disease using amyloid PET scans. There is a lack of standardization in the interpretation of amyloid PET scans. Different imaging centres may use different imaging protocols and analysis techniques, which can affect the accuracy and reliability of the results. This can lead to variability in the diagnosis and treatment of Alzheimer's disease. The visual assessment used for Amyloid PET positivity classification also depends on the experience of the reader. Prognosis can be confirmed when there is a system that aids in the diagnosis of amyloid positive and negative images and SUVR quantification automatically.

Recently machine learning and deep learning techniques are used for amyloid analysis based on different radiotracers like Florbetapir, Florbetaben, and Flutemetamol. The amyloid status study of 18^{F}-Florbetaben images is done by a deep learning network for cardiac amyloidosis classification [39]. Machine learning techniques Gradient Boosting Machine and Random Forest are used to predict the Aβ positivity in Aβ PET images using cerebral microbleeds features [40]. Another study utilizes deep learning techniques to find the amyloid PET positivity classification using FDG PET images [41]. In previous work, the 3D CNN model is trained on a local dataset and tested on ADNI 18^{F}-Florbetaben images to determine the amyloid positive or negative class [42]. Some studies used Res-Net to classify the amyloid status in florbetapir images from the ADNI dataset [35,43]. In [44], the authors used RegNet X064 with a gradient boosting decision tree for predicting SUVR.

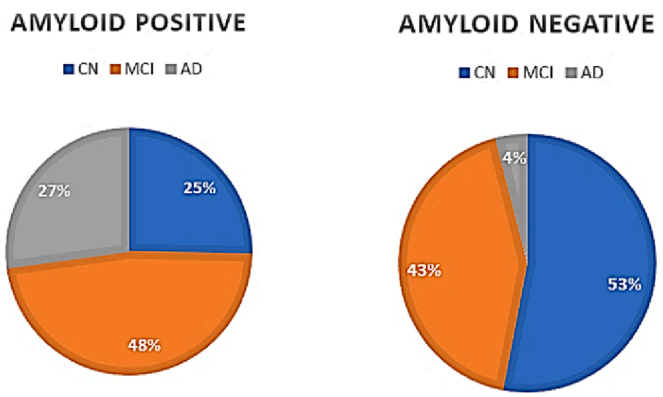

Fig. 1. Percentage of participants in amyloid positive and negative category.

Even though various techniques are introduced by researchers to perform amyloid analysis, still there is a need to improve the classification process. The purpose of this work is to design a deep learning model with better performance than the current systems available to detect the amyloid burden in the brain using Florbetapir scans. In addition to the amyloid positivity classification, it would be informative to know the amount of SUVR quantification while developing a deep learning model. Florbetapir PET images are frequently used in the molecular imaging of neurodegeneration patients. These scans are used to detect beta-amyloid plaque deposits in the human brain. There is a strong need for a system that helps in the automatic standard uptake value ratio (SUVR) quantification of Florbetapir PET images which is otherwise a lengthy process where manual errors could occur at many stages. Hence, a deep learning system with attention is proposed that could help in the quantification process which will act as an aid to radiologists and neurologists. It is inspired by the attention mechanism used in medical image analysis [45–47] for classification or segmentation due to its capability to identify disease-affected regions. The channel attention and the spatial attention used in the proposed model utilize the inter-spatial relationship of features and channel information to have better feature descriptors for SUVR quantification. The model is developed based on a large dataset of Florbetapir PET scans from Alzheimer Disease Neuroimaging Initiative (ADNI) and also tested on another dataset of Florbetapir PET scans from Anti-Amyloid Treatment in Asymptomatic Alzheimer's (A4) study. A Graphical User Interface (GUI) is designed for amyloid analysis of Florbetapir PET scans based on the proposed attention-based model. This work will act as a major step toward the applicability of artificial intelligence in amyloid PET SUVR quantification.

2. Methods

2.1. Study participants

Amyloid PET data taken from Alzheimer Disease Neuroimaging Initiative (ADNI) (https://adni.loni.usc.edu) database and Anti-Amyloid

2. a) Amyloid Positive Scan

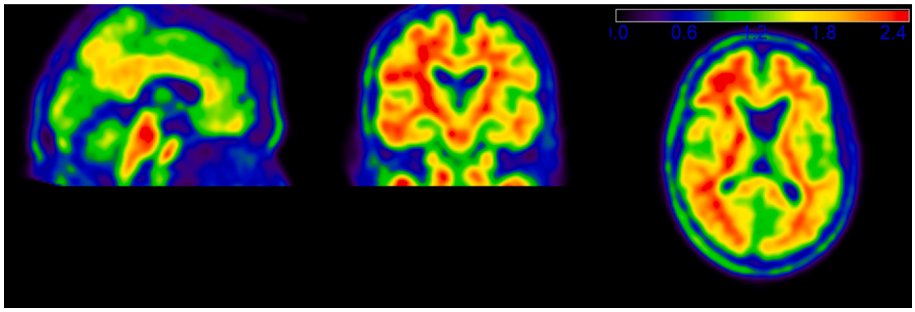

2. b) Amyloid Negative Scan

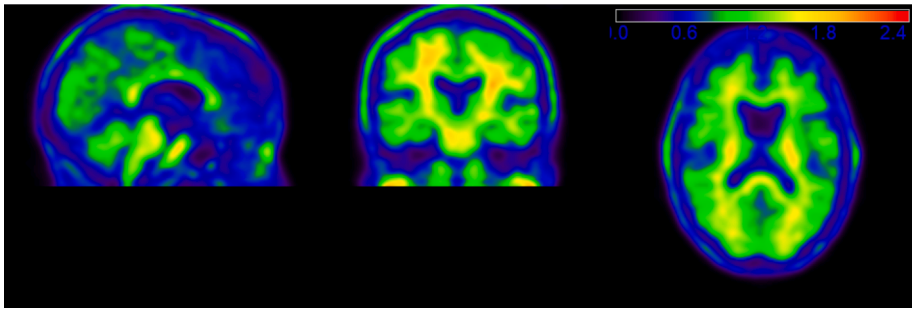

Fig. 2. Sample scans considered in this study a) Amyloid Positive Scan b) Amyloid Negative Scan.

Treatment in Asymptomatic Alzheimer's (A4) study [48] are used in the preparation of this article. A total of 2647 florbetapir PET scans are taken from ADNI1, ADNI2, ADNIGO, and ADNI3 participants. The data include longitudinal ^{18}F[AV-45] scan images of cognitive normal (CN), Mild Cognitive Impairment (MCI), and Alzheimer's Disease (AD) participants. The gender and age criteria of the participants involved in the ADNI clinical trial are shown in Table1 and the percentage of participants in amyloid positive and amyloid negative classification are shown in Fig. 1..

A total of 1413 Florbetapir scans are taken from three research groups – elevated amyloid level group, not elevated amyloid level group belonging to Longitudinal Evaluation of Amyloid Risk and Neurodegeneration (LEARN) observation, and not elevated amyloid level group not belonging to LEARN observation from A4 study to further test the model. Out of these 489 scans belong to amyloid positive scans and 924 scans belong to amyloid negative scans. The amyloid positive scans belong to 300 female subjects and 189 male subjects involved in the A4 study. The amyloid negative scans belong to 545 female subjects and 379 male subjects from the A4 study. The mean age of amyloid positive participants' category is 72.23 with a standard deviation of 5.16 and the mean age of amyloid negative participants' category is 71.22 with a standard deviation of 4.59.

2.2. PET scans

The scans are downloaded from the ADNI database (adni.loni.usc.edu/methods/pet-analysis/pre-processing) in NIFTI format. They have a uniform size of 160x160x96. Initially, the AC-PC line is adjusted for each scan and then the ^{18}F-florbetapir template [49] is used for the normalization of the PET scan. These steps are performed using Statistical Parametric Mapping SPM12 (http://www.fil.ion.ucl.ac.uk/spm/) added to the MATLAB R2020b. The normalized volumes are of size 101x116x96 with a voxel size of 2x2x2mm^3.

Florbetapir PET scans from the A4 study were acquired 50–70 min' post-injection and reconstructed in 4x5-minute frames as NIFTI files. These amyloid PET scans from the A4 study have different volume sizes. AC-PC line is adjusted for each Florbetapir PET scan and the scan is normalized to the PET template [49] to have processed volumes of size 101x116x96 with a voxel size of 2x2x2 mm^3. An example of amyloid positive scan and amyloid negative scan in sagittal, coronal, and axial view considered in this study is shown in Fig. 2.

Standardized Uptake Value Ratios (SUVRs) are obtained for all the scans from UC Berkeley ^{18}F-florbetapir analysis data of the ADNI dataset (ida.loni.usc.edu). SUMMARYSUVR_COMPOSITE_REFNORM SUVR is used for the proposed analysis because longitudinal Florbetapir PET scans are considered (ida.loni.usc.edu). For the A4 study, SUVRs based on whole cerebellum cut-off 1.11 is obtained. The linear regression equation given by eq.1 is used for converting SUVR based on the whole cerebellum to SUVR based on the composite reference region by Florbetapir (AV45) processing methods (http://adni.loni.usc.edu).

$$y = 0.630x + 0.080 \tag{1}$$

where x represents the SUVR based on the whole cerebellum and y represents the SUVR based on the composite region.

In order to obtain SUVR from the amyloid PET scan, many computations are carried out. It involves registering the PET image to the nearby time MRI image of the same patient, segmenting both the brain images correctly, and then calculating uptake values in these corresponding segmented regions of the grey matter, and then normalizing these values according to the white matter region uptake and other small areas in the brain. Hence, to avoid these complex tasks, a deep learning system is proposed which can automate this task.

2.3. Proposed work

The florbetapir PET images that are normalized to the PET template [49] are chosen as input images. The proposed work consists of training a classification model first and then using it further to train a regression model for SUVR quantification. The proposed work is given in two steps.

1. Initially, 3D CNN with an attention module is designed to provide better accuracy in classifying amyloid-positive images from amyloid-negative images. 3D CNN is used because it will be able to acquire

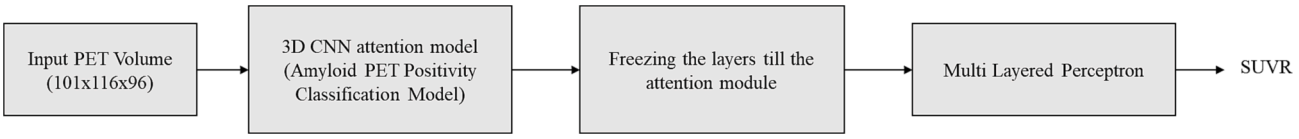

Fig. 3. Workflow in training the 3D CNN-based regression model.

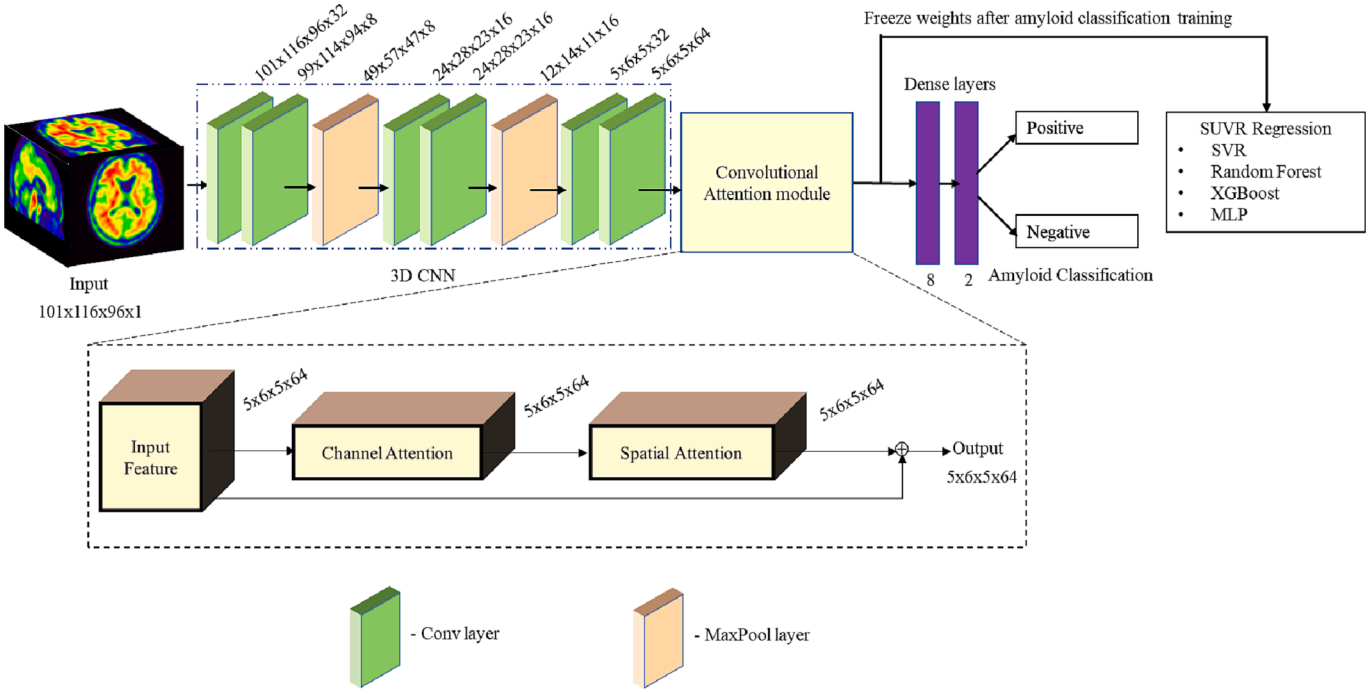

Fig. 4. Illustration of the proposed 3D CNN model with a convolutional block attention module.

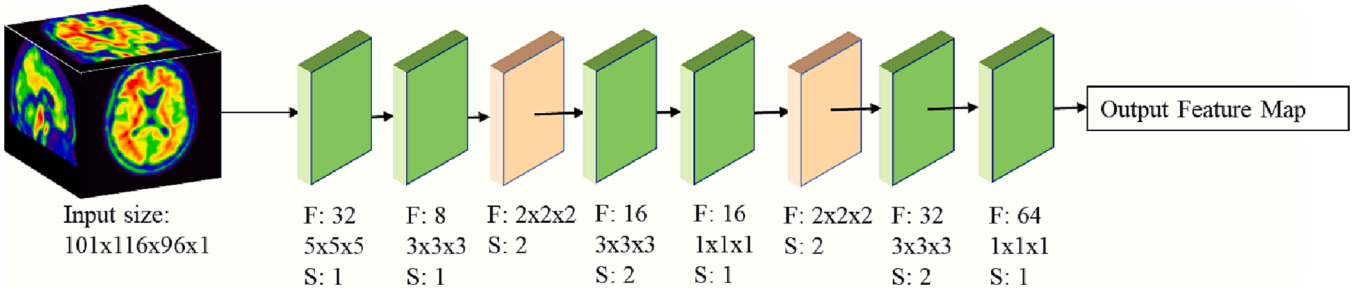

Fig. 5. 3D CNN module with filters specification.

better spatial information when compared to 2D CNN. The convolutional block attention module helps in gaining both channel-related information as well as spatial information so as to obtain a good feature set.

2. After freezing the weights of the above-mentioned classification model, features from the attention block are used to develop a regression model further to predict the SUVR values. These information-rich features are given as input to different machine learning models and multi-layered perceptron to check which model will better quantify SUVR. When 3D CNN with attention module is used directly for SUVR quantification, instead of amyloid positivity classification, it resulted in high RMSE and MAE values for SUVR. Hence, these two steps are used while modeling the system to predict SUVR.

The workflow is depicted in Fig. 3.

2.4. 3D CNN module

The architecture of the proposed convolutional block attention-based 3D convolutional neural network is shown in Fig. 4.

The ^{18}F-Florbetapir PET scans each of size 101x116x96x1 from the training set of ADNI are used as input to the 3D CNN. The 3D CNN module consists of convolution blocks made up of 3D convolution kernels and MaxPooling blocks. The 3D CNN module along with the filters specification is expressed in Fig. 5.

The batch Normalization layer and ReLU activation layer follow after every convolutional layer. The number of filters for the convolution blocks are 32, 8, 16, 16, 32, and 64 respectively. The size of the kernels in the first convolution layer is 5x5x5. The size of the kernels for the second, third, and fifth convolution layers are 3x3x3 and for the fourth and sixth layers are 1x1x1. The stride value is 1 for all the convolution layers except the third and fifth convolutional layer which has the stride

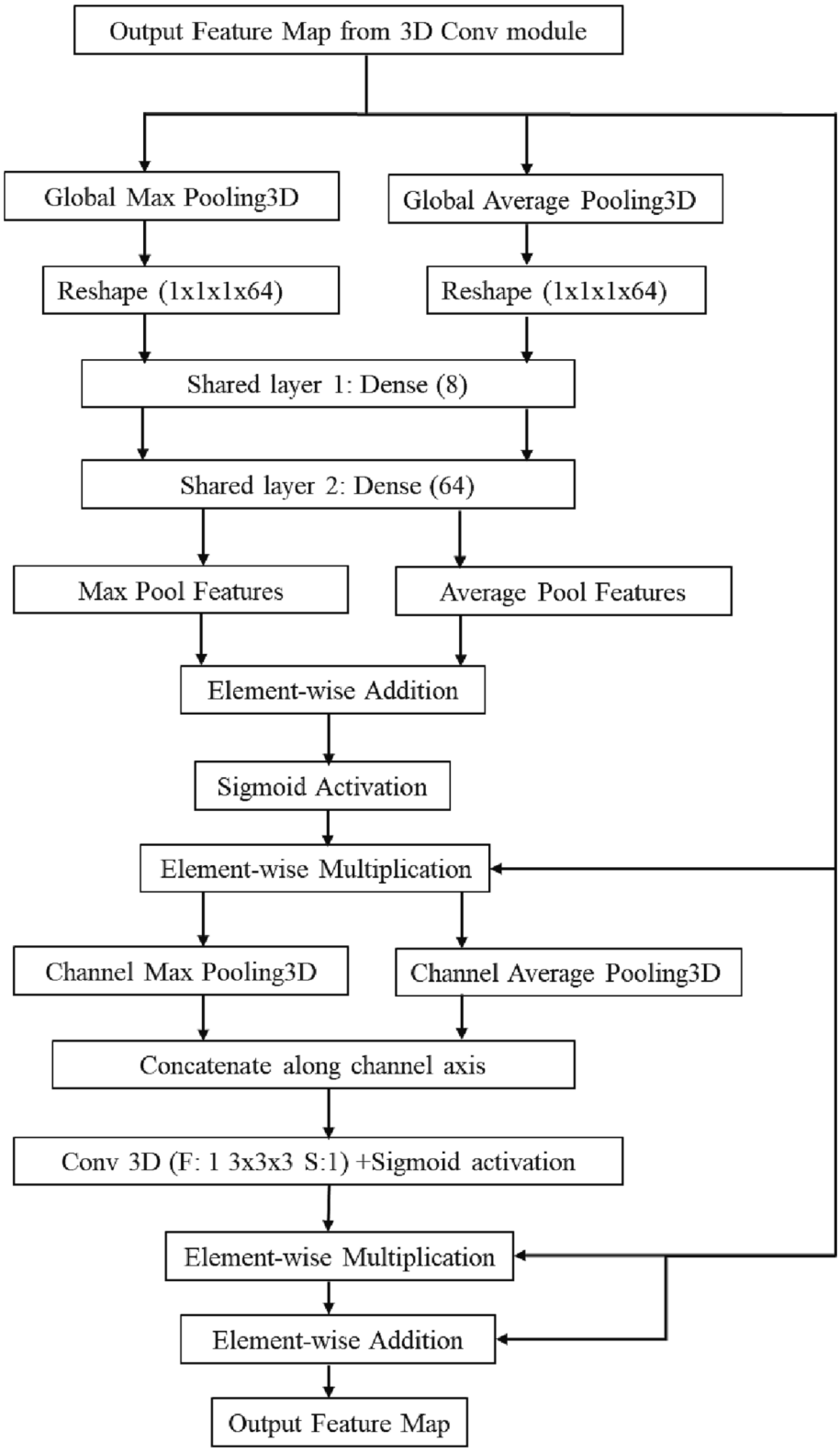

Fig. 6. 3D Attention module with detailed operation.

value of 2. MaxPooling uses a kernel size of 2x2x2 with stride 2 in all directions. The initializer used in the convolution layer is the He-Normal initializer [50]. The output features from this 3D CNN backbone are given as input to the convolutional attention block module.

2.4.1. Convolutional block attention module

When humans are viewing any object, they will give attention to certain regions of the object to understand the object. The convolutional block attention module follows this concept by capturing the essential information of the images [51]. This concept was designed for 2D CNN-based models. This is adapted to work with 3D CNN in the proposed

work. The convolutional block attention module consists of channel attention followed by spatial attention.

For computing channel attention spatial dimension is squeezed, global max-pooling (GMP) and global average pooling (GAP) are performed and passed onto the shared multi-layered perceptron (MLP). The sigmoid activation function (σ) is used at its output. The channel attention is computed using the formula in eq.2.

$$Channel\ \ Attention = \sigma(MLP(GMP) \oplus MLP(GAP)) \tag{2}$$

For computing spatial attention, channel max-pooling (CMP) and channel average pooling (CAP) are concatenated and given as input to the convolution layer with a single 3x3x3 kernel, stride 1, and same padding which is passed on to the sigmoid activation (σ) layer. The spatial attention is computed using the formula in eq. (3).

$$Spatial\ \ Attention(SA) = \sigma(conv[CMP; CAP])) \tag{3}$$

The output of the attention block is obtained by the elementwise addition of the input to the attention block and the output of the spatial attention map. The proposed attention module based on 3D input is shown in Fig. 6.

The output from the convolutional block attention module is flattened and given as input to a dense layer with RELU activation followed by a dense layer with softmax activation function for amyloid positive and negative classification.

2.4.2. MLP regressor

MLP regressor consists of two dense layers with eight and single neurons respectively. To prevent overfitting of the model, dropout of 0.2 is used. Adam optimizer is used in the training of the model with an initial learning rate of 0.001. The output from the convolutional block attention module is given as input to the MLP regressor.

2.4.3. Other regressors

Apart from MLP, other regressors like support vector regressor (SVR), extreme gradient boost (XGBoost) regressor), and light gradient boosted machine (LGBM) regressor are modelled with the features from the attention block as input.

Support vector regression is obtained with the help of the non-linear Gaussian kernel function. The gaussian kernel function is given by Eq. (4).

$$f(x_i, x_j) = exp(\gamma \|x_i - x_j\|^2), \quad \gamma > 0 \tag{4}$$

where the dot product of x_i, x_j is calculated by using the Euclidean distance in the original space and gamma (γ) is a controlling parameter to avoid the model to overfit or underfit. XGBoost Regressor and LGBM Regressor, gradient boosting algorithms based on decision trees are also tested upon the features obtained from the attention block.

2.5. Performance metrics

RMSE and mean absolute value errors (MAE) are evaluated upon the predicted SUVR and the original SUVR obtained from the quantification based on MRI images. RMSE and MAE metrics explain the amount of deviation from the original SUVR. RMSE and MAE are calculated using Eq. (5) and Eq. (6).

$$RMSE = \sqrt{\frac{\sum (y_i - y_{pred})^2}{n}} \tag{5}$$

$$MAE = \frac{|y_i - y_{pred}|}{n} \tag{6}$$

where y_i represents the actual values and y_{pred} represents the predicted values and n is the number of observations.

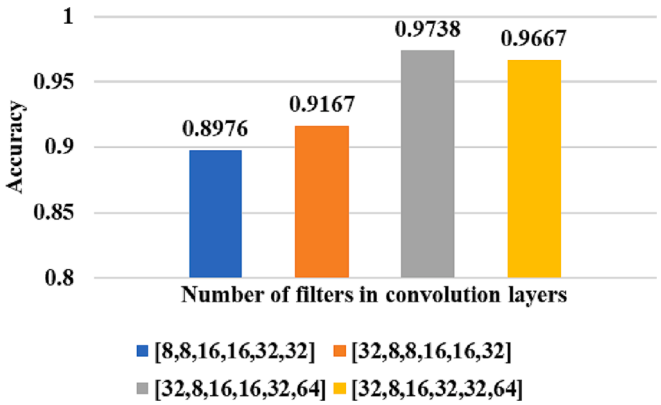

Fig. 7. Validation performance of the model with various filters of convolution layers.

3. Results and discussion

A total of 2116 longitudinal Florbetapir PET images which consists of 80% of total scans from ADNI are used for training and validating the model. A hold-out test set of 531 Florbetapir images (the remaining 20% of ADNI scans) are used to evaluate the trained model. Patient-wise splitting of longitudinal PET data is performed so that no data leakage occurs during the training, validation, and testing phases. It is difficult to store the entire PET image data in RAM. Hence, TensorFlow records are used for batch processing of the PET volumes. Data augmentation is performed over the training set by flipping the hemispheres of the brain. The categorical loss function is used for training the initial model for amyloid positive and amyloid negative classification. Early stopping is used during training to monitor the validation loss with the patience of 15 epochs. The learning rate starts from 0.001 and is reduced by a factor of 0.1 till it reaches 1E-5 when the validation loss does not decrease for 10 epochs. The proposed model is implemented with TensorFlow and Keras framework using Google Colaboratory (GPU: 1xTesla K80).

Different validation runs are carried out by choosing the filters for the convolution layers as [8,8,16,16,32,32], [32,8,8,16,16,32], [32,8,16,16,32,64], [32,8,16,32,32,64] which is depicted in Fig. 7.

The model when validated using only the 3D CNN backbone resulted in an accuracy of 0.9595. For spatial attention alone, kernel sizes of 5 and 7 are used for different validation runs resulting in an accuracy of 0.9619 and 0.9643 respectively. For channel attention alone, channel ratio of 8 and 16 resulted in an accuracy of 0.9630 and 0.9574 respectively. 3D CNN having channel attention with a channel ratio of 8, and spatial attention with a kernel size of 7 resulted in an accuracy of 0.9738 respectively which is depicted in Fig. 8.

Based on these results, the model with [32,8,16,16,32,64] filters for the convolution layers consisting of spatial and channel attention with a kernel size of 7 is chosen to be the best model for classification. 5-fold cross-validation is performed based on this model with accuracy as the performance metric. An accuracy of 0.9709 ± 0.002 is achieved upon 5-fold cross-validation. In order to ensure no data leakage occurs, the split is made in such a way that the scans of a particular person belong completely in each fold and are not split across folds. The training time took nearly three hours and is performed for 38 epochs. Testing was completed within a few seconds upon running a model on the Colab environment with GPU. The hold-out test dataset is used only after the finalization of the model selection and completion of hyperparameter tuning. The proposed 3D CNN model with attention block for amyloid positivity classification results in an accuracy of 0.9699, a sensitivity of 0.9720, and a specificity of 0.9680 on the test dataset from ADNI. Florbetapir PET scans of Alzheimer's disease are classified with better accuracy than the scans of the subjects belonging to mild cognitive impairment or normal controls.

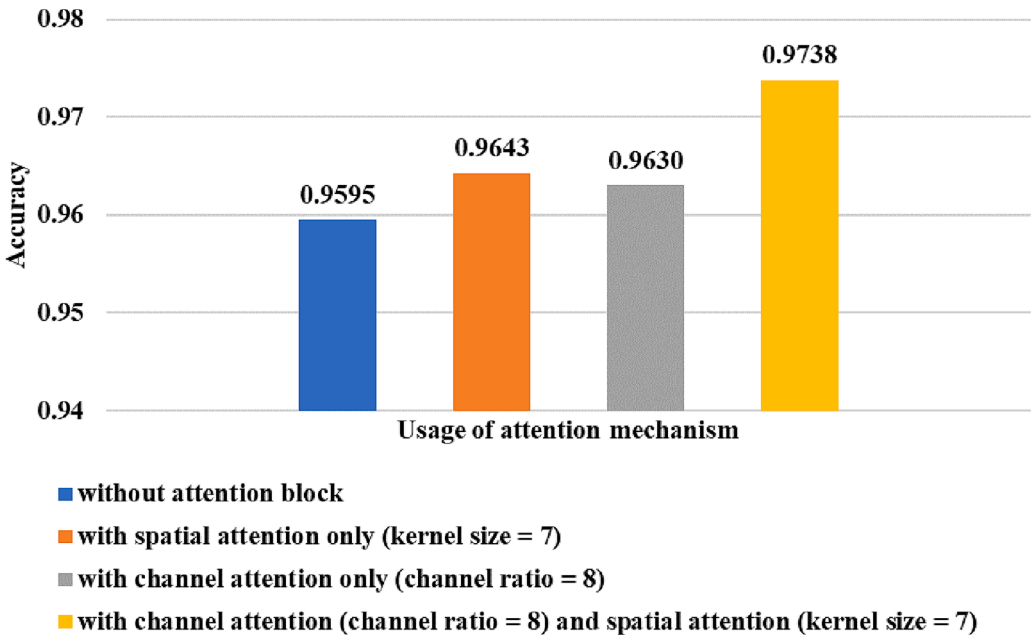

Fig. 8. Validation performance of the CNN model with and without attention.

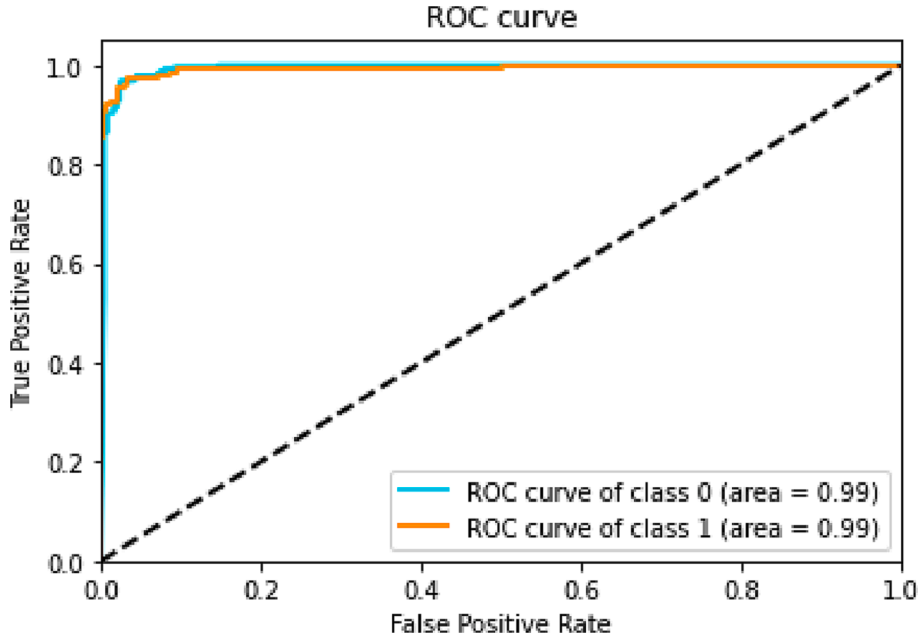

Fig. 9. ROC curve for the ADNI test data.

ROC curve is constructed based on true positive rate and false-positive rate for both the classes (amyloid positive and negative). It tells how good the model is at classifying each class. The ROC curve and AUC are shown in Fig. 9.

The chosen classification model resulted in a confusion matrix for the test data from ADNI as shown in Table 2. As can be perceived from Table 2, nine amyloid negative scans are misinterpreted as positive scans and seven amyloid positive scans are misinterpreted as negative scans, and all the remaining scans are correctly classified.

Gradient-weighted class activation mapping (Grad-CAM) was introduced to create visual elucidations for the decisions taken by the 2D convolutional neural network [52]. Grad-CAM highlights the important regions in the image used for identifying the image as belonging to a particular class. Based on this method, Grad-CAM is adapted for the 3D convolutional neural network using the gradients of the last layer before flattening layer of the proposed model. Grad-CAM result is displayed for a random slice of each axis in Fig. 10 for a particular PET scan which is amyloid positive.

As shown in Fig. 10, Grad-CAM method is implemented for 3D CNN with attention block to illuminate the model-interested regions of amyloid positive scan. It shows the regions used by the 3D CNN with attention block to determine the scan to be positive. The Grad-CAM of the proposed model also indicates that the model is performing its intended work instead of looking at random locations to determine the amyloid positivity.

Hence, the chosen classification model weights are frozen. Next, the features from the attention block are extracted and given as input to another MLP having two dense layers with 8 and single neurons

Table 2
Confusion matrix for test data from ADNI.

Disease category	Confusion matrix	
AD (n = 84)	TP = 71	FP = 1
Amyloid positive: n = 72		
Amyloid negative: n = 12		
	FN = 1	TN = 11
MCI (n = 267)	TP = 119	FP = 3
Amyloid positive: n = 122		
Amyloid negative: n = 145		
	FN = 3	TN = 142
CN (n = 180)	TP = 53	FP = 5
Amyloid positive: n = 56		
Amyloid negative: n = 124		
	FN = 3	TN = 119

respectively. By freezing the model layers as input, the regressor layers are designed. root mean squared error (RMSE) loss is used to train the model and RMSE is used as the metric to be displayed after every epoch while model training takes place. When the validation loss remains the same and does not decrease, the learning rate is reduced by a factor of 0.1 till it reaches 1E-5. The model is saved at the end of every epoch. An early stopping mechanism is used to stop the training of the model if the validation loss does not decrease for 25 epochs. The proposed model is developed using TensorFlow and Keras using Google Colaboratory with a GPU runtime (1xTesla K80). Increasing the number of neurons or layers did not improve the performance of the model. Increasing or decreasing the dropout rate also did not increase the performance of the model.

Other regressor models are developed with the help of scikit-learn, XGBoost, and LGBM libraries. The models are validated with different parameter values for C and gamma for SVR. Similarly, for XGBoost different values are given for n_estimators, max_depth, learning rate, subsample, and colsample_bytree and tested. For the LGBM regressor, the objective is set to be RMSE, and different values are given to learning rate, reg_lambda, n_estimators, colsample_bytree, max_depth, num_leaves, subsample, and subsample_freq and all the models are evaluated. Table 3. shows the best regressor models developed from the SVR, XGBoost, LGBM regressors, and MLP regressor with dropout which are evaluated against the validation data. For SVR, 0.1 is used for the parameter C value. For XGB Regressor, n_estimators are chosen to be 1000, with max_depth as 7, subsample as 0.7, and colsample_bytree as 0.8. Similarly, for LGBM regressor, learning rate is chosen as 0.08, reg_lambda value is chosen as 0.1, n_estimators as 600, colsample_bytree as 0.8, max_depth as 5, num_leaves as 10, subsample as 0.8, and subsample_freq as 15.

Based on the results seen in Table 3, the 3D CNN attention-based

Table 3
Validation Performance of SUVR regression by the different models by freezing the weights of the classification model.

Model	RMSE	MAE
SVR	0.0681	0.0586
XGBoost Regressor	0.0411	0.0318
LGBM Regressor	0.0386	0.0296
Proposed MLP	0.0315	0.0260

Table 4
Performance of different models on ADNI test data.

Model	Total number of parameters present in the model	FLOPs	Memory	RMSE on ADNI Test data	MAE on ADNI Test data
ResNet50	23,620,481	2.13G	90.38 MB	0.0794	0.0595
ResNet101	42,690,945	4.26G	163.3 MB	0.0722	0.0559
ResNet152	58,403,713	6.32G	223.5 MB	0.0666	0.0504
VGG19	20,028,993	8.75G	76.4 MB	0.1488	0.1293
Reith F et al. (2020) [35]	–	–	–	0.059 ± 0.005	–
Reith F et al. (2021) [43]	–	–	–	0.0339 ± 0.0003	–
Maddury S et al. (2023) [44]	–	–	–	–	0.0441
Proposed CNN model with attention blocks	109,935	23.9G	479 KB	0.0362	0.0260

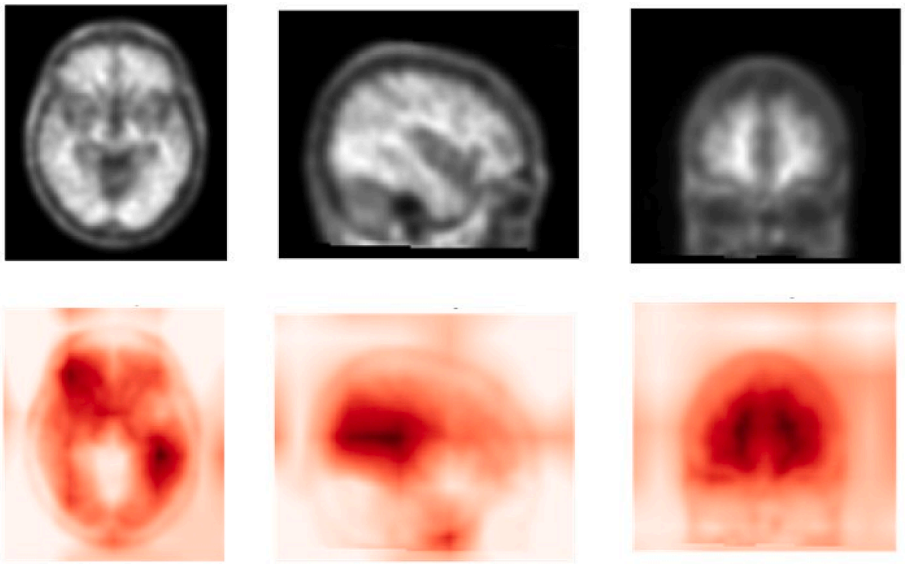

Fig. 10. Axial, sagittal and coronal slices of Florbetapir image is displayed in grayscale in top row and Grad-CAM overlayed on axial, sagittal and coronal slices of the same Florbetapir image in bottom row.

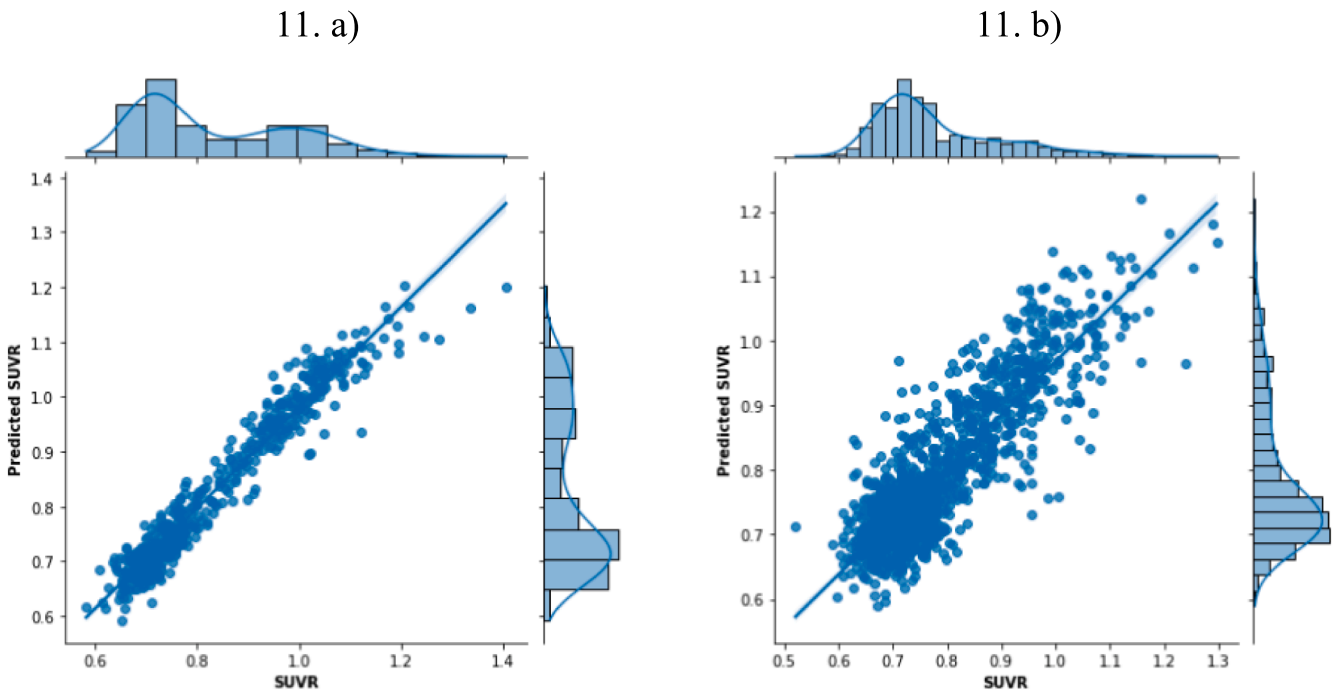

Fig. 11. Scatter Plot of SUVR and predicted SUVR with their corresponding histograms on a) ADNI test data b) A4 study test data.

model with MLP is selected as the final model and tested upon the separate hold-out test data. Testing is completed within a few seconds in GPU runtime of the Google Colab environment. The model is evaluated on the test set only after the final selection of the model with the desired parameters. The proposed 3D CNN attention-based model achieved RMSE of 0.0362 and MAE of 0.026 on the ADNI test data.

The proposed 3D CNN attention-based model with MLP for SUVR regression is compared with the ResNet and VGG-19 models designed using transfer learning by fine-tuning ResNet and VGG-19 weights that were pre-trained by using the ImageNet dataset of natural images in Table 4. From Table 4, it is observed that both RMSE and MAE are the lowest for the proposed 3D CNN attention-based model when compared with the other models. Among the 96 slices of the scans, the slices numbered 40, 50, and 60 are used as input to the ResNet and VGG19 models whereas the entire volume of the scan 101x116x96 is given as input to the proposed model. Hence 3D convolutions are not used for ResNet and VGG19 models because the scan slices are not adjacent. The proposed model also has less number of parameters when compared to other models and therefore it occupies less storage space but provides better results. This is because, for the calculation of SUVR in PET scans, different brain regions (frontal region, lateral temporal region, parietal region and cingulate region) are considered which may not be the case when only 3 slices in the brain region are taken. Though, the proposed model performs better than the compared models it has more floating-point operations (FLOPs) when compared with the other models because it is based on 3D volumes instead of 2D images. Henceforth, work will also be done in the future to reduce the number of FLOPs and also to further improve the performance of the model.

The proposed 3D CNN attention-based model is checked for its performance by comparing it with other recent studies. In [41], deep learning-based amyloid positivity classification is performed using FDG PET images. This resulted in an accuracy of 0.770, sensitivity of 0.800, and specificity of 0.740 in the internally validated dataset. In [53], the training was performed on a local dataset using a 3D CNN model and tested on ADNI 18^{F}-Florbetaben images. This resulted in an accuracy of 0.92 when tested over the ADNI dataset.

In [35], ResNet architectures were used with 3 slices to perform classification with a mean accuracy of 0.9388, mean sensitivity of 0.9152, and mean specificity of 0.9623. SUMMARYSUVR_WHOLECEREBNORM SUVR from the ADNI website was evaluated based on the model [35] and found to have a mean RMSE score of 0.059 upon cross-validation. In [43], ResNet combined with gradient boosting tree was used with 3 input slices and 8 clinical features which resulted in a mean RMSE score of 0.0339 upon cross-validation. In [44], the authors used RegNet X064 and gradient boosting tree with 3 slices as input to achieve MAE of 0.0441. The proposed 3D CNN with an attention block model (classification model) with a five-fold cross validation accuracy of 0.9709 ± 0.002 resulting in an accuracy of 0.9699, a sensitivity of 0.9720, and a specificity of 0.9680 on the hold-out ADNI test data is used for the initial layers of the regressor model for SUVR quantification. The proposed model 3D CNN with attention outperformed the existing models as well as all the slices are considered instead of some specific slices to determine amyloid positivity. Hence the proposed model has better features derived from the amyloid positivity classification model. In addition to this, a separate hold-out test set is considered apart from the cross-validation test data. Consequently, this helped to achieve better performance in the regression model for SUVR quantification when compared with the recent studies. SUMMARYSUVR_COMPOSITE_REFNORM SUVR from the ADNI website is detected with RMSE of 0.0362 and MAE of 0.026 on the ADNI test data. Since longitudinal data is considered, SUMMARYSUVR_COMPOSITE_REFNORM SUVR is used as mentioned on the LONI IDA website repository. R^2 score of 0.94 on the ADNI test data set indicates a high correlation between the original SUVR and predicted SUVR. When this attention-based model is tested on A4 study dataset, it resulted in RMSE of 0.058 and an MAE of 0.044. R^2 score of 0.8 is achieved on the A4 study dataset. Henceforth, work will be done in the future to improve the performance on both ADNI and A4 study datasets and also to reduce the number of FLOPs to further improve the performance of the model for SUVR quantification.

The scatter plot of the original SUVR values and the predicted SUVR values and their corresponding distributions are displayed in Fig. 11. From this plot, the predicted SUVR is seen highly correlating with the actual SUVR derived based on the MRI scans for ADNI dataset when compared to A4 study dataset.

The longitudinal Florbetapir PET images from the ADNI dataset

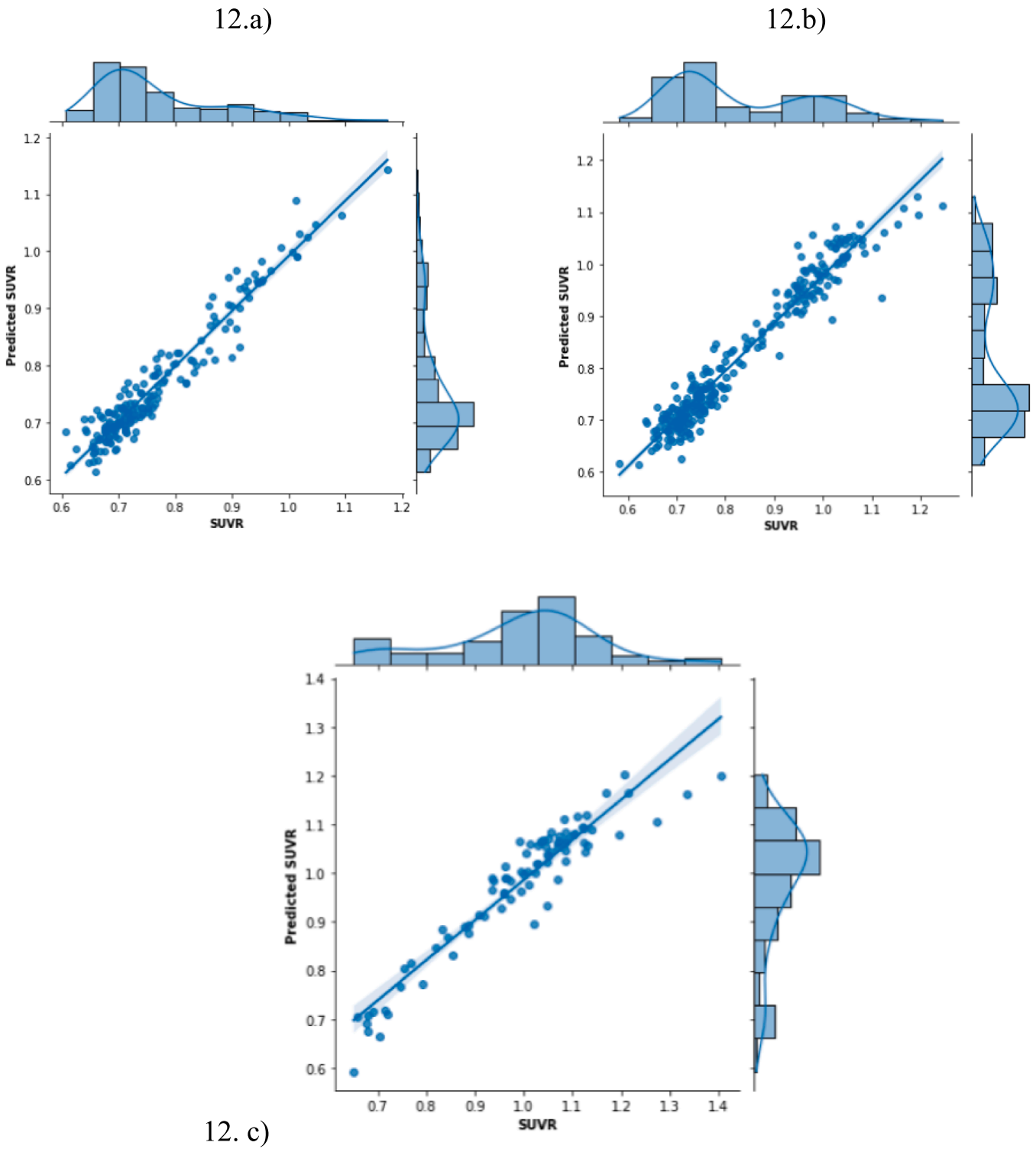

Fig. 12. Scatter plots of original and predicted SUVR with their corresponding histograms for a) Normal Controls category b) MCI category c) AD category.

contains participants belonging to CN, MCI, and AD disease category. The training, validation, and test data set contains images Florbetapir PET images from all the disease categories. For the various disease stages, the performance of the proposed 3D CNN attention-based model for the test data is shown in Fig. 12. The predicted SUVR is found to be highly correlated with the actual SUVR for all three categories.

In this work, the amyloid SUVR quantification of Florbetapir PET images is carried out. The evaluation metrics proved that the proposed 3D CNN attention-based model is a robust model. Based on this proposed work, a graphical user interface (GUI) is created. The GUI is designed so that users who want to know the value of SUVR quantification of a patient's Florbetapir PET image can simply upload the file into the system. By using this GUI, the image file can be easily selected by clicking on the button that says 'Choose file'. The GUI is designed for selecting only NIFTI image files. Another button named 'Quantify' is designed to predict the SUVR of amyloid PET images based on the proposed 3D CNN with attention module and MLP. This graphical user interface is shown in Fig. 13. The screen of the graphical user interface is split into two such

13.a)

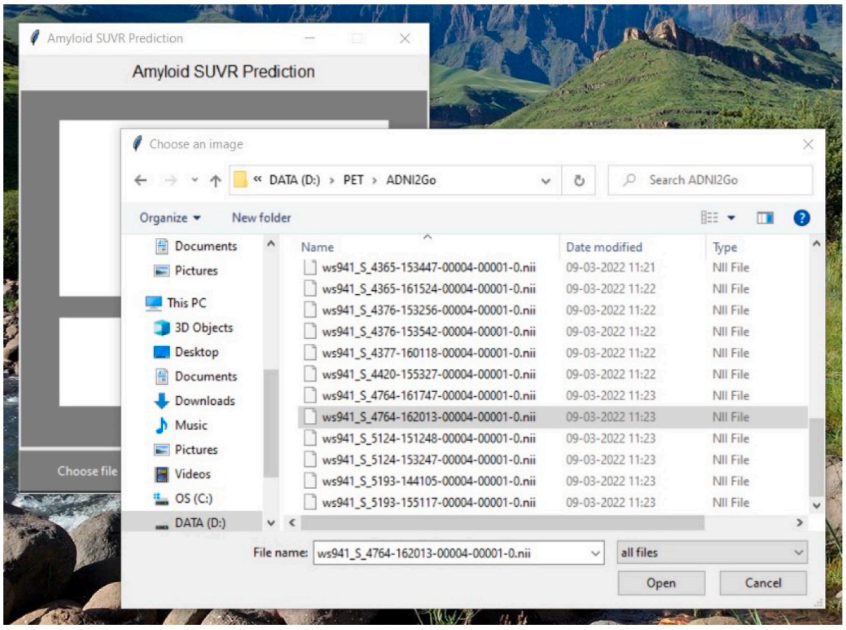

13.b)

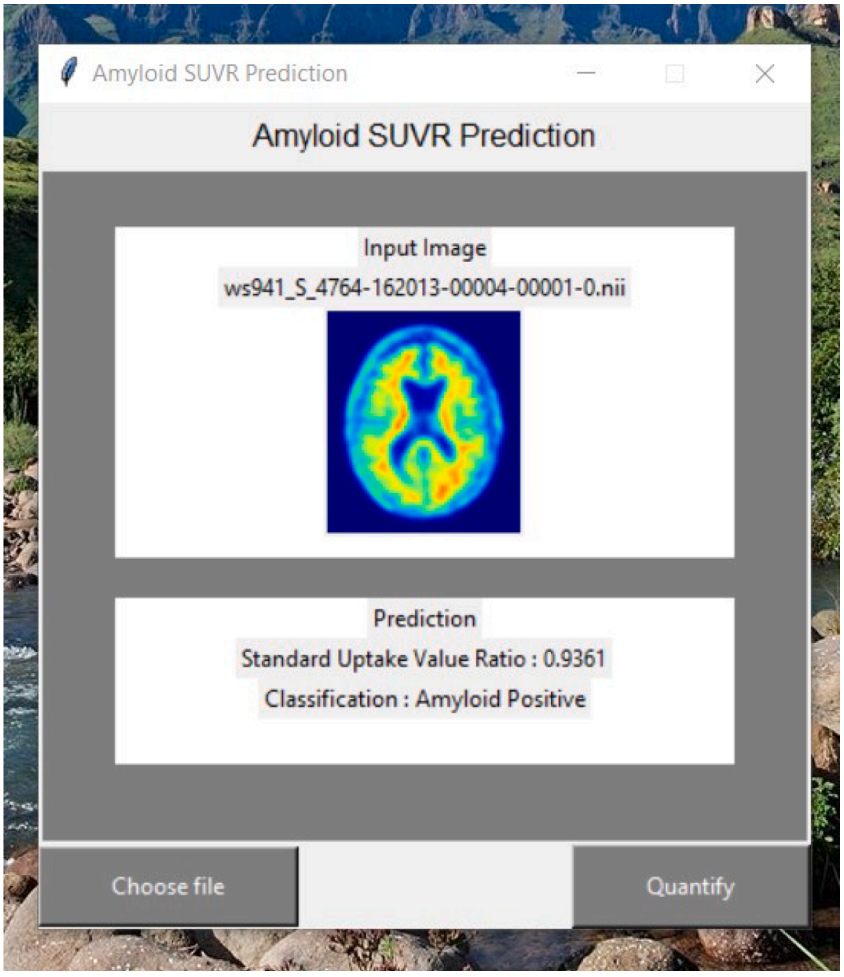

Fig. 13. Graphical User Interface a) Selecting the input Florbetapir PET NIFTI file b) Predicted output.

that the top window of the screen displays a single slice of the Florbetapir PET input image from the chosen NIFTI file. The bottom window displays the SUVR prediction and tells the user whether the input image is amyloid positive or amyloid negative. Thus, the GUI design will be an easy tool to operate for any person with little computer knowledge.

4. Conclusion

Advancement in molecular PET imaging allows for better visualization of beta-amyloid deposits in the brain. Florbetapir tracer has a very high potential for quick and early detection of amyloid deposition which could aid in targeted treatments. Deep learning is currently used in medicinal practice for chest X-ray detection. Soon there will be a period when deep learning will be used in all fields of medicine. The proposed model will act as a small step toward using deep learning in the field of amyloid quantification in the living human brain. The proposed CNN with an attention-based model shows the predicted SUVRs are in accordance with the amyloid estimation done based on MRI images of the ADNI dataset with an R^2 score of 0.94 and the A4 study dataset with an R^2 score of 0.8. The proposed model works the best on ADNI and there is some slight deviation in its performance when considering the A4 study. Similarly, when the PET scans are considered from other scanning centres, there might be a little deviation in SUVR quantification which could be overcome by transfer learning on sample scans from those scanning centres. The proposed model will thus aid in the automatic standard uptake value ratio quantification. The GUI developed along with the proposed model will make it easier to use by clinicians to aid in their assessment. In the future, work will be carried out to check whether this model could be applied to other amyloid PET scans with different radiopharmaceuticals. In addition to this, a deep learning model for SUVR quantification across different brain regions would be carried out with a lesser number of FLOPs that occupies small memory space to assist the radiologists. When SUVR is detected over different brain regions then that could lead to the beginning of an era of targeted medicines for amyloid pathology in neurodegenerative diseases. The targeted drugs will become a possible cure for the chronic Alzheimer's disease-affected subjects.

5. Ethical approval.

Approval for the ADNI protocol has been granted by the institutional review board at the study sites.

6. Consent for publication

All the authors agreed to the publication of the article.

7. Availability of supporting data/Data availability

Data used in the current study were collected by ADNI. Data has been downloaded through the LONI platform after approval by the data access committee of ADNI. Data can only be accessed from ADNI and cannot be shared.

Funding

This research did not receive any specific grant from funding agencies in the public, commercial, or not-for-profit sectors.

Declaration of Competing Interest

The authors declare that they have no known competing financial interests or personal relationships that could have appeared to influence the work reported in this paper.

Data availability

The data that has been used is confidential.

Acknowledgments

Data used in the preparation of this article were obtained from the Alzheimer's Disease Neuroimaging Initiative (ADNI) database (adni.loni.usc.edu). Data collection and sharing for this project were funded by the Alzheimer's Disease Neuroimaging Initiative (ADNI) (National Institutes of Health Grant U01 AG024904) and DOD ADNI (Department of Defense award number W81XWH-12-2-0012). ADNI data are disseminated by the Laboratory for Neuro Imaging at the University of Southern California.

References

[1] L.-F. Lue, L. Brachova, W.H. Civin, J. Rogers, Inflammation, Aβ Deposition, and Neurofibrillary Tangle Formation as Correlates of Alzheimer's Disease Neurodegeneration, J. Neuropathol. Exp. Neurol. 55 (1996) 1083–1088, https://doi.org/10.1097/00005072-199655100-00008.
[2] P.-F. D'Haese, M. Ranjan, A. Song, et al., β-Amyloid Plaque Reduction in the Hippocampus After Focused Ultrasound-Induced Blood-Brain Barrier Opening in Alzheimer's Disease, Front. Hum. Neurosci. 14 (2020).
[3] P.H. Dinh, A novel approach based on Three-scale image decomposition and Marine predators algorithm for multi-modal medical image fusion, Biomed. Signal Process. Control 67 (2021), 102536, https://doi.org/10.1016/J.BSPC.2021.102536.
[4] P.H. Dinh, An improved medical image synthesis approach based on marine predators algorithm and maximum Gabor energy, Neural Comput. Appl. 34 (2022) 4367–4385, https://doi.org/10.1007/S00521-021-06577-4.
[5] P.H. Dinh, A novel approach using structure tensor for medical image fusion, Multidimens Syst. Signal Process 33 (2022) 1001–1021, https://doi.org/10.1007/S11045-022-00829-9.
[6] P.-H. Dinh, A novel approach using the local energy function and its variations for medical image fusion, 2023, https://doi.org/101080/13682199202321909471–17. https://doi.org/10.1080/13682199.2023.2190947.
[7] P.H. Dinh, N.L. Giang, A new medical image enhancement algorithm using adaptive parameters, Int. J. Imaging Syst. Technol. 32 (2022) 2198–2218, https://doi.org/10.1002/IMA.22778.
[8] P.-H. Dinh, A Novel Approach Based on Marine Predators Algorithm for Medical Image Enhancement, Sens. Imaging 24 (2023) 1–23, https://doi.org/10.1007/S11220-023-00411-Y.
[9] R. Ramya, K. Mala, S. Selva Nidhyananthan, 3D Facial Expression Recognition Using Multi-channel Deep Learning Framework, Circuits Syst. Signal Process 39 (2020) 789–804, https://doi.org/10.1007/s00034-019-01144-8.
[10] T. Manonmani, V. Pushparaj, Trail optimization framework to detect nonlinear object motion in video sequences, Signal Image Video Process 14 (2020) 537–545, https://doi.org/10.1007/s11760-019-01581-7.
[11] N.S. Russel, A. Selvaraj, Robust affect analysis using committee of deep convolutional neural networks, Neural Comput. Appl. 34 (2022) 3633–3645, https://doi.org/10.1007/s00521-021-06632-0.
[12] K. Asghar, X. Sun, P.L. Rosin, et al., Edge–texture feature-based image forgery detection with cross-dataset evaluation, Mach. Vis. Appl. 30 (2019) 1243–1262, https://doi.org/10.1007/s00138-019-01048-2.
[13] Y. Fu, X. Ma, H. Zhou, Automatic detection of multi-crossing crack defects in multicrystalline solar cells based on machine vision, Mach. Vis. Appl. 32 (2021) 60, https://doi.org/10.1007/s00138-021-01183-9.
[14] S. Yao, J. Tan, Y. Chen, Y. Gu, A weighted feature transfer gan for medical image synthesis, Mach. Vis. Appl. 32 (2020) 22, https://doi.org/10.1007/s00138-020-01152-8.
[15] E. Amrutha, S. Arivazhagan, W. Sylvia Lilly Jebarani, MixNet: A Robust Mixture of Convolutional Neural Networks as Feature Extractors to Detect Stego Images Created by Content-Adaptive Steganography, Neural Process. Lett. 54 (2022) 853–870, https://doi.org/10.1007/s11063-021-10661-0.
[16] C. Strathearn, E.M. Ma, A Novel Speech to Mouth Articulation System for Realistic Humanoid Robots, J. Intell. Rob. Syst. 101 (2021) 54, https://doi.org/10.1007/s10846-021-01332-2.
[17] S. Zhang, J. Yao, R. Wang, et al., Design of intelligent fire-fighting robot based on multi-sensor fusion and experimental study on fire scene patrol, Rob. Auton. Syst. 154 (2022), 104122, https://doi.org/10.1016/j.robot.2022.104122.
[18] D.C. Araújo, A.A. Veloso, R.S. de Oliveira Filho, et al., Finding reduced Raman spectroscopy fingerprint of skin samples for melanoma diagnosis through machine learning, Artif. Intell. Med. 120 (2021), 102161, https://doi.org/10.1016/j.artmed.2021.102161.
[19] P.H. Dinh, A novel approach based on Grasshopper optimization algorithm for medical image fusion, Expert Syst. Appl. 171 (2021), 114576, https://doi.org/10.1016/J.ESWA.2021.114576.
[20] P.H. Dinh, Medical image fusion based on enhanced three-layer image decomposition and Chameleon swarm algorithm, Biomed. Signal Process. Control 84 (2023), 104740, https://doi.org/10.1016/J.BSPC.2023.104740.

[21] P.H. Dinh, Combining spectral total variation with dynamic threshold neural P systems for medical image fusion, Biomed. Signal Process. Control 80 (2023), 104343, https://doi.org/10.1016/J.BSPC.2022.104343.
[22] P.H. Dinh, Combining Gabor energy with equilibrium optimizer algorithm for multi-modality medical image fusion, Biomed. Signal Process. Control 68 (2021), 102696, https://doi.org/10.1016/J.BSPC.2021.102696.
[23] P.H. Dinh, Multi-modal medical image fusion based on equilibrium optimizer algorithm and local energy functions, Appl. Intell. 51 (2021) 8416–8431, https://doi.org/10.1007/S10489-021-02282-W.
[24] G.R. Hemalakshmi, D. Santhi, V.R.S. Mani, et al., Classification of retinal fundus image using MS-DRLBP features and CNN-RBF classifier, J. Ambient Intell. Hum. Comput. 12 (2021) 8747–8762, https://doi.org/10.1007/s12652-020-02647-y.
[25] C. Sarasaen, S. Chatterjee, M. Breitkopf, et al., Fine-tuning deep learning model parameters for improved super-resolution of dynamic MRI with prior-knowledge, Artif. Intell. Med. 121 (2021), 102196, https://doi.org/10.1016/j.artmed.2021.102196.
[26] T. Kaur, T.K. Gandhi, Deep convolutional neural networks with transfer learning for automated brain image classification, Mach. Vis. Appl. 31 (2020) 20, https://doi.org/10.1007/s00138-020-01069-2.
[27] N.S. Punn, S. Agarwal, RCA-IUnet: a residual cross-spatial attention-guided inception U-Net model for tumor segmentation in breast ultrasound imaging, Mach. Vis. Appl. 33 (2022) 27, https://doi.org/10.1007/s00138-022-01280-3.
[28] R. Divya, R. Shantha Selva Kumari, Initiative the ADN, Genetic algorithm with logistic regression feature selection for Alzheimer's disease classification, Neural Comput. Appl. 33 (2021) 8435–8444, https://doi.org/10.1007/s00521-020-05596-x.
[29] S. Basheera, M. Satya Sai Ram, A novel CNN based Alzheimer's disease classification using hybrid enhanced ICA segmented gray matter of MRI, Comput. Med. Imaging Graph. 81 (2020), 101713, https://doi.org/10.1016/j.compmedimag.2020.101713.
[30] M. Liu, F. Li, H. Yan, et al., A multi-model deep convolutional neural network for automatic hippocampus segmentation and classification in Alzheimer's disease, Neuroimage 208 (2020), 116459, https://doi.org/10.1016/j.neuroimage.2019.116459.
[31] S. Spasov, L. Passamonti, A. Duggento, et al., A parameter-efficient deep learning approach to predict conversion from mild cognitive impairment to Alzheimer's disease, Neuroimage 189 (2019) 276–287, https://doi.org/10.1016/j.neuroimage.2019.01.031.
[32] Z. Peng, M. Ni, H. Shan, et al., Feasibility evaluation of PET scan-time reduction for diagnosing amyloid-β levels in Alzheimer's disease patients using a deep-learning-based denoising algorithm, Comput. Biol. Med. 138 (2021), 104919, https://doi.org/10.1016/j.compbiomed.2021.104919.
[33] K.T. Chen, O. Adeyeri, T.N. Toueg, et al., Investigating Simultaneity for Deep Learning-Enhanced Actual Ultra-Low-Dose Amyloid PET/MR Imaging, Am. J. Neuroradiol. (2022), https://doi.org/10.3174/ajnr.A7410.
[34] B.M. de Vries, S.S.V. Golla, J. Ebenau, et al., Classification of negative and positive 18F-florbetapir brain PET studies in subjective cognitive decline patients using a convolutional neural network, Eur. J. Nucl. Med. Mol. Imaging 48 (2021) 721–728, https://doi.org/10.1007/s00259-020-05006-3.
[35] F. Reith, M.E. Koran, G. Davidzon, G. Zaharchuk, Application of deep learning to predict standardized uptake value ratio and amyloid status on 18F-florbetapir PET using ADNI data, Am. J. Neuroradiol. 41 (2020) 980–986, https://doi.org/10.3174/ajnr.A6573.
[36] F. Liu, S. Yuan, W. Li, et al., Patch-based deep multi-modal learning framework for Alzheimer's disease diagnosis using multi-view neuroimaging, Biomed. Signal Process. Control 80 (2023), 104400, https://doi.org/10.1016/J.BSPC.2022.104400.
[37] V.P. Subramanyam Rallabandi, K. Seetharaman, Deep learning-based classification of healthy aging controls, mild cognitive impairment and Alzheimer's disease using fusion of MRI-PET imaging, Biomed. Signal Process. Control 80 (2023), 104312, https://doi.org/10.1016/J.BSPC.2022.104312.
[38] A.J. Aschenbrenner, B.A. Gordon, T.L.S. Benzinger, et al., Influence of tau PET, amyloid PET, and hippocampal volume on cognition in Alzheimer disease, Neurology 91 (2018) e859.
[39] M.F. Santarelli, D. Genovesi, V. Positano, et al., Deep-learning-based cardiac amyloidosis classification from early acquired pet images, Int. J. Cardiovasc. Imaging 37 (2021) 2327–2335, https://doi.org/10.1007/s10554-021-02190-7.
[40] Y.H. Jung, H. Lee, H.J. Kim, et al., Prediction of amyloid β PET positivity using machine learning in patients with suspected cerebral amyloid angiopathy markers, Sci. Rep. 10 (2020) 18806, https://doi.org/10.1038/s41598-020-75664-8.
[41] S. Kim, P. Lee, K.T. Oh, et al., Deep learning-based amyloid PET positivity classification model in the Alzheimer's disease continuum by using 2-[18F]FDG PET, EJNMMI Res. 11 (2021), https://doi.org/10.1186/s13550-021-00798-3.
[42] S.Y. Lee, H. Kang, J.H. Jeong, D.Y. Kang, Performance evaluation in [18F] Florbetaben brain PET images classification using 3D Convolutional Neural Network, PLoS One 16 (2021), https://doi.org/10.1371/journal.pone.0258214.
[43] F.H. Reith, E.C. Mormino, G. Zaharchuk, Predicting future amyloid biomarkers in dementia patients with machine learning to improve clinical trial patient selection, Alzheimer's & Dementia (New York, N Y) 7 (2021) e12212.
[44] S. Maddury, K. Desai, DeepAD: A deep learning application for predicting amyloid standardized uptake value ratio through PET for Alzheimer's prognosis, Front. Artif. Intell. 6 (2023) 4, https://doi.org/10.3389/FRAI.2023.1091506.
[45] L. Li, M. Xu, H. Liu, et al., A Large-Scale Database and a CNN Model for Attention-Based Glaucoma Detection, IEEE Trans. Med. Imaging 39 (2020) 413–424, https://doi.org/10.1109/TMI.2019.2927226.
[46] N. Yamanakkanavar, B. Lee, A novel M-SegNet with global attention CNN architecture for automatic segmentation of brain MRI, Comput. Biol. Med. 136 (2021), 104761, https://doi.org/10.1016/j.compbiomed.2021.104761.
[47] X. Sun, P. Garg, S. Plein, R.J. van der Geest, SAUN: Stack attention U-Net for left ventricle segmentation from cardiac cine magnetic resonance imaging, Med. Phys. 48 (2021) 1750–1763, https://doi.org/10.1002/mp.14752.
[48] R.A. Sperling, M.C. Donohue, R. Raman, et al., Association of Factors With Elevated Amyloid Burden in Clinically Normal Older Individuals, JAMA Neurol. 77 (2020) 735–745, https://doi.org/10.1001/jamaneurol.2020.0387.
[49] L. Iaccarino, R. la Joie, R. Koeppe, et al., rPOP: Robust PET-only processing of community acquired heterogeneous amyloid-PET data, Neuroimage 246 (2022), 118775, https://doi.org/10.1016/j.neuroimage.2021.118775.
[50] K. He, X. Zhang, S. Ren, J. Sun, Delving Deep into Rectifiers: Surpassing Human-Level Performance on ImageNet Classification, in: 2015 IEEE International Conference on Computer Vision (ICCV), 2015, pp 1026–1034.
[51] S. Woo, J. Park, J.-Y. Lee, I.S. Kweon, CBAM: Convolutional Block Attention Module, in: V. Ferrari, M. Hebert, C. Sminchisescu, Y. Weiss (Eds.), Computer Vision – ECCV 2018, Springer International Publishing, Cham, 2018, pp. 3–19.
[52] R.R. Selvaraju, M. Cogswell, A. Das, et al., Grad-CAM: Visual Explanations from Deep Networks via Gradient-Based Localization, in: 2017 IEEE International Conference on Computer Vision (ICCV), 2017, pp. 618–626.
[53] S.-Y. Lee, H. Kang, J.-H. Jeong, D. Kang, Performance evaluation in [18F] Florbetaben brain PET images classification using 3D Convolutional Neural Network, PLoS One 16 (2021) e0258214.